ARTICLE

Chinese Journal of Structural Chemistry

Construction of Z-Scheme In_2S_3-TiO_2 for CO_2 Reduction under Concentrated Natural Sunlight

Ya Liu[1]*, Fangbo Yu[1], Feng Wang[1], Shengjie Bai[1] and Guiwei He[1]

[1]*State Key Laboratory of Multiphase Flow in Power Engineering, Xi'an Jiaotong University, Xi'an 710049, China*

ABSTRACT Producing chemical fuels from sunlight enables a sustainable way for energy consumption. Among various solar fuel generation approaches, photocatalytic CO_2 reduction has the advantages of simple structure, mild reaction condition, directly reducing carbon emissions, etc. However, most of the current photocatalytic systems can only absorb the UV-visible spectrum of solar light. Therefore, finding a way to utilize infrared light in the photocatalytic system has attracted more and more attention. Here, a Z-scheme In_2S_3-TiO_2 was constructed for CO_2 reduction under concentrated natural sunlight. The infrared light was used to create a high-temperature environment for photocatalytic reactions. The evolution rates of H_2, CO, and C_2H_5OH reached 262.2, 73.9, and 27.56 μmol·h^{-1}·g^{-1}, respectively, with an overall solar to fuels efficiency of 0.002%. This work provides a composite photocatalyst towards the utilization of full solar light spectrum, and could promote the research on photocatalytic CO_2 reduction.

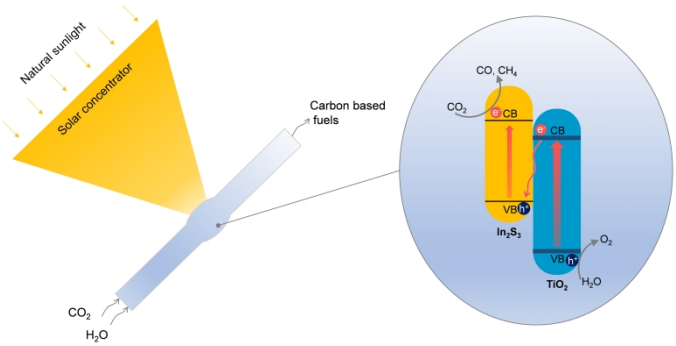

Keywords: solar energy, CO_2, In_2S_3, TiO_2

n INTRODUNTION

With the rapid growth of the global economy and energy demand, environmental issues caused by carbon emissions become more and more serious at present. Photocatalytic CO_2 reduction (CO_2R) is a clean technology to produce chemical fuels and could reduce carbon emissions directly.[1] Within this technology, H_2O and CO_2 are reduced to small molecules, such as CO, CH_4, C_2H_4, CH_3OH, and C_2H_5OH.[2,3] In the past few decades, various photocatalytic systems have been reported for producing carbon-based fuels.[4–6] The manufacture simulated sunlights, such as mercury and xenon lamps, are typically used as the light source to drive photocatalytic reactions in labs.[7–10] However, those simulated sunlights are greatly differing from natural sunlight in the spectrum, especially in the infrared spectral range. Hence, conducting photocatalytic solar fuel generation under natural sunlight has great practical significance.

The energy of the solar-generated electrons is limited to the band structure of the photocatalysts.[11–14] Only the UV-visible spectrum of the solar light can be absorbed in most of the published photocatalytic systems.[15] It is notable that, infrared light makes up 49.4% of the total solar radiation on the earth's surface. In our opinion, compared to UV-visible light based photocatalytic systems, the ones driven by full solar light spectrum would provide a way to increase the energy efficiency of solar to fuel. In general, there are mainly three ways to use infrared light in the photocatalytic system for CO_2R, including photocatalysis,[16,17] thermal catalysis,[18] and photo-thermal catalysis.[19,20]

In practice, infrared light needs to be concentrated to promote photocatalytic reaction by generating energetic electrons or creating a high temperature for chemical reactions. At present, only a few published photocatalytic CO_2R systems were driven by concentrated natural sunlight directly. For instance, Fe_2O_3/Fe_3O_4 has been used as the catalyst in a photocatalytic CO_2R that was illuminated by tracing natural sunlight.[21] The reaction temperature is ranged from 400 to 680 °C. The maximum production rates of CH_4, C_2H_4, and C_2H_6 were 1470.7, 736.2, and 277.2 μmol·h^{-1}·g^{-1}, respectively. However, the solar to fuel efficiency was only 0.0022% at 560 °C. Moreover, a TiO_2 based photocatalytic system was also measured under natural sunlight.[22] The production rates of CH_4, C_2H_4, and C_2H_6 reached 1578.60, 289.22 and 673.02 μmol·h^{-1}·g^{-1}, respectively (531 °C, 1.0 MPa). The overall solar to fuel efficiency reached 0.15%.

Both Fe_2O_3/Fe_3O_4 and TiO_2 in the above studies show relatively low activities. The solar to fuel efficiency and stability of the current photocatalytic CO_2R systems need to be improved urgently. It is of great significance to put more testing effort into natural sunlight driven photocatalytic CO_2R systems, and further reveal the photocatalytic mechanism, especially on the function of infrared photons.

Herein, we try to build a Z-scheme photocatalytic CO_2R system that aimed to broaden the light absorption to the infrared range and simultaneously provide enough photovoltage for CO_2R. We have noticed that the band alignment In_2S_3-TiO_2 is quite suitable for photocatalytic reactions.[23,24] Within this heterojunction, TiO_2 has a relatively wide bandgap and can supply enough photovoltage for CO_2R, but only utilizes UV light.[25,26] As a contrast, with a relatively narrow bandgap, In_2S_3 can utilize sunlight from ultraviolet to the near-infrared range and promote the effective use of light generated carriers.[27,28] Also, the conduction band of In_2S_3 is around –0.98 eV,[29,30] which is much higher than that of TiO_2 (–0.42 eV[31,32]). As it is known, the higher conduction band enables moving the electrons to a higher energy level, and thus presents a higher capability to drive the chemical reactions. For instance, a type II In_2S_3/TiO_2

DOI: 10.14102/j.cnki.0254-5861.2021-0046

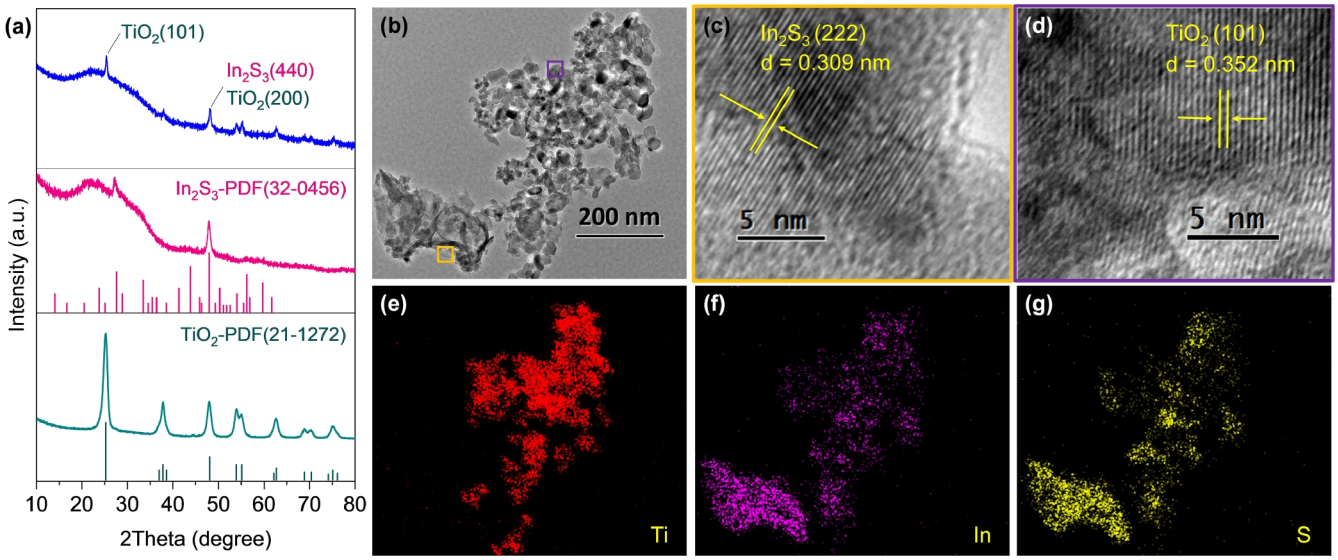

Figure 1. Structural and morphological characterization. (a) XRD pattern of the as-prepared samples. Vertical drop lines indicate the Powder Diffraction Files (PDF) of In_2S_3 and TiO_2. (b) TEM image of the as-prepared In_2S_3-TiO_2. HRTEM images of the selected area in (b): (c) orange frame in (b) and (d) purple frame in (b). The EDX mapping analysis of In_2S_3-TiO_2 for (e) Ti, (f) In, and (g) S.

heterojunction was constructed from TiO_2 nanosheets by Huang and coworkers for photocatalytic CO_2R, which showed a superior CH_4 production rate of 16.21 $\mu mol \cdot h^{-1} \cdot g^{-1}$ without any sacrificial agent.[33] However, at present, the published In_2S_3/TiO_2 photocatalysts were only tested under simulated sunlight for solar fuel generation. In this work, we fabricated TiO_2-In_2S_3 heterojunction from commercial TiO_2. The structural and optical properties of this composite photocatalyst are presented. The photocatalytic CO_2R is conducted under concentrated natural sunlight directly.

n RESULTS AND DISCUSSION

In_2S_3-TiO_2. XRD pattern was used to study the crystal structure of the as-prepared samples (Figure 1a). All of the peaks from TiO_2 are in good agreement with the standard card (PDF: 21-1272), which indicates an anatase crystal structure. The two peaks from In_2S_3, 27.5º and 47.9º, are in good agreement with the standard card (PDF: 32-0456), which indicates the as-prepared In_2S_3 is β-In_2S_3 with a cubic structure.[34] For as-prepared In_2S_3-TiO_2, the peak around 25.3° corresponds to anatase TiO_2(101). Considering the TiO_2 used here doesn't have preferential orientation, the intensity of TiO_2(200) should be close to 48% of TiO_2(101). However, the intensity of obtained peak at ~48° is close to the peak around 25.3°. Therefore, we believe that TiO_2(200) overlaps with In_2S_3(440) at $2\theta \approx 48°$.

The SEM images of the as-prepared samples (Figure S1) show that TiO_2 is nanoparticles in the diameter of 15–35 nm, and In_2S_3 has a morphology of "nanoflowers". However, we didn't get a clear structure of In_2S_3-TiO_2 from the SEM image (Figure S1c). The TEM images and EDX mappings of In_2S_3-TiO_2 are also measured to further confirm the crystal structures, as shown in Figure 1b–1g. We can find that the diameter of anatase is about 20–50 nm on the top right corner and the In_2S_3 sheet is on the bottom left corner through a comparison of the TEM image (Figure 1b) and EDX mappings (Figure 1e to Figure 1f). In the In_2S_3 area (Figure 1c), we find a crystalline interplanar space of 0.309 nm, which corresponds to the (222) face. In the TiO_2 area (Figure 1d), we find a crystalline interplanar space of 0.352 nm, which corresponds to the (101) face. We didn't find any crystalline interplanar space of anatase in the In_2S_3 area.

To determine the existence and valence states of elements, XPS spectra of In_2S_3-TiO_2 composite were also conducted. The survey-scan XPS spectrum (Figure S2) clearly shows the characteristic peaks of Ti 2*p*, O 1*s*, In 3*d*, and S 2*p*, which correspond to the elecments in TiO_2 and In_2S_3. The two peaks of Ti $2p_{3/2}$ and Ti $2p_{1/2}$ at 458.5 and 464.3 eV confirm that the valence state of Ti is tetravalent, as shown in Figure 2a[35]. The two peaks of In 3*d* at 452.2 and 444.7 eV (Figure 2b) correspond to In $3d_{3/2}$ and In $3d_{5/2}$.[36] Two peaks of S 2*p* at 161.4 and 162.6 eV (Figure 2c) correspond to S $2p_{3/2}$ and S $2p_{1/2}$, respectively.[30] Furthermore, the O 1*s* peaks (Figure 2c) observed at 529.8 eV are attributed to the lattice oxygen of TiO_2. Another two peaks at 531.6 and 533.2 eV are attributed to the surface hydroxyl groups and physically adsorbed oxygen, respectively.[37,38] All these XPS results confirm the coexistence of In_2S_3 and TiO_2 in the composite samples.

Photocatalytic CO_2 Reduction. Before measuring the photocatalytic CO_2R under natural light directly, we firstly studied the performance under simulated sunlight. Figure 3a indicates that In_2S_3-TiO_2 performed best at 170 ºC for producing CO with an evolution rate of 7.1 $\mu mol \cdot h^{-1} \cdot g^{-1}$. However, CO almost reduced to zero in the last 2 hours when the temperature reached 250 ºC, due to the inactivation of photocatalyst. Of interest, no H_2 was detected below 150 ºC. The higher the temperature was, the more H_2 was produced. Moreover, the photocatalytic CO_2R performance of In_2S_3 and TiO_2 was also measured under simulated sunlight at 170 ºC. As shown in Figure 3b, there were no products detected from In_2S_3. TiO_2 performs better than In_2S_3-TiO_2 for H_2 evolution. Only In_2S_3-TiO_2 produced CO. These results indicate that In_2S_3 and TiO_2 should

DOI: 10.14102/j.cnki.0254-5861.2021-0046

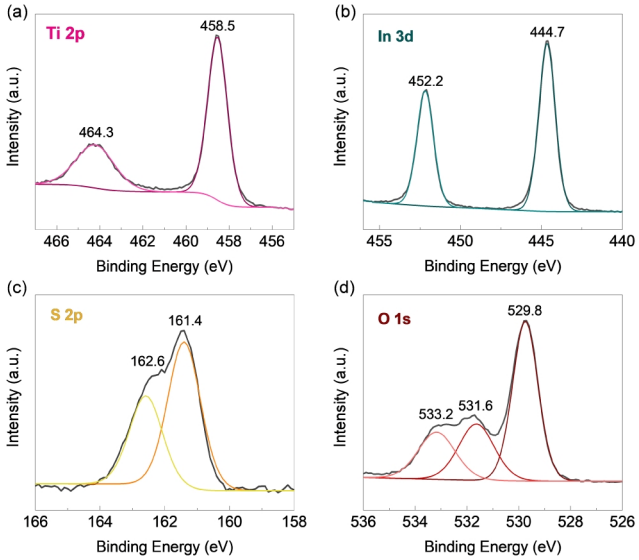

Figure 2. High-resolution XPS spectra of In_2S_3-TiO_2. (a) Ti 2*p*, (b) In 3*d*, (c) S 2*p*, and (d) O 1*s*.

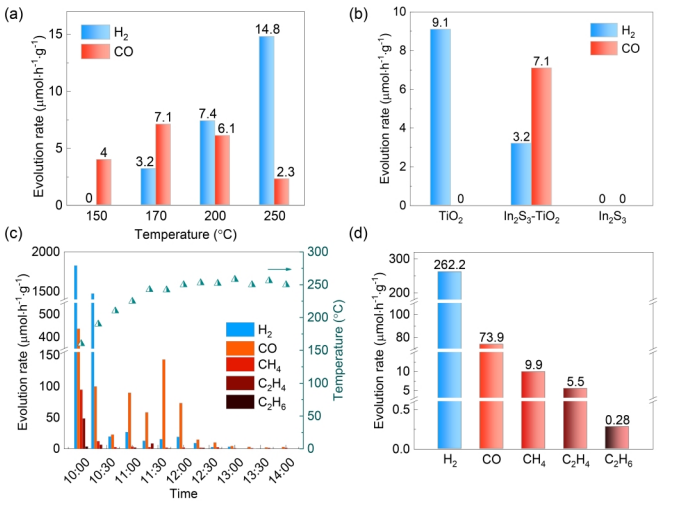

Figure 3. Evolution rates of chemical fuels. (a) In_2S_3-TiO_2 at different temperatures under simulated sunlight. (b) In_2S_3-TiO_2, In_2S_3, and TiO_2 at 170 ºC under simulated sunlight. (c) In_2S_3-TiO_2 under natural sunlight, a sunny day in Xi'an city. (d) The average evolution rates of the produced chemical fuels, which are calculated based on the data in (c).

be combined for reducing CO_2 to CO. Moreover, the enhanced photocurrent density in J-V curves and smaller arc radius in the electrical impedance spectroscopy diagram indicate the as-prepared In_2S_3-TiO_2 has a better charge separation efficiency and lower charge transfer resistance than TiO_2 and In_2S_3, as shown in Figure S3.

Under natural sunlight, infrared radiation was used to create a high-temperature environment for photocatalytic CO_2R reactions. As shown in Figure 3c, the temperature of the reactor was quickly moved up by more than 150 ºC. The detected gas products of photocatalytic CO_2R include H_2, CO, CH_4, C_2H_4, and C_2H_6. The CO_2R activity is very high during the first hour of reaction. The maximum evolution rate for producing H_2, CO, CH_4, and C_2H_4 reached 1820, 435, 94, and 48 $\mu mol \cdot h^{-1} \cdot g^{-1}$, respectively. As time went on, the temperature rises to the deactivation temperature of catalyst, 250 ºC, corresponding to the results measured under simulated light. In addition, Figure 3d shows that the average evolution rate of H_2 is much higher than that of carbon-based fuels. The solar to fuels efficiency was also calculated, ~0.002% for all of the chemical fuels, ~0.00148% for carbon-based fuels, which is much lower than the results measured under simulated light. Of particular note is that liquid product, ethanol, was detected under natural sunlight, which is quite different from the measurements under simulated sunlight. After 4 hours' photocatalytic reaction, 2 mL of condensate aqueous ethanol solution with a concentration of 1.05 mmol/L was collected, corresponding to 27.56 $\mu mol \cdot h^{-1} \cdot g^{-1}$.

The stability of the as-prepared In_2S_3-TiO_2 was also evaluated (Figure S4). Although the photocatalytic CO_2R performance decreased at each cycle, the photocatalyst can be regenerated *via* a sample drying process. Therefore, we further believe that the deactivation of In_2S_3/TiO_2 in Figure 3c comes from the changes of the chemical reaction sites, which may be blocked by the adsorbed molecules.

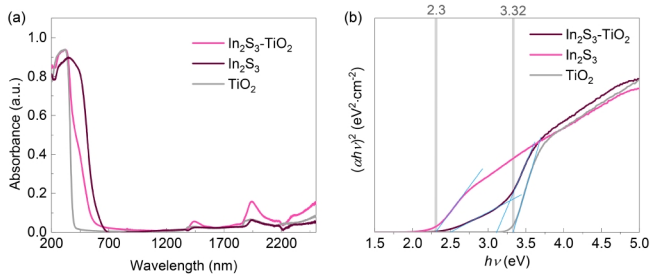

Figure 4. (a) UV-Vis-NIR spectral and (b) $(ahv)^2$ versus photon energy curves of In_2S_3-TiO_2, In_2S_3, and TiO_2.

Optical Properties and Reaction Mechanism. It can be seen from Figure 4a that the absorbance of In_2S_3-TiO_2 within the UV-Vis range is located between In_2S_3 and TiO_2. However, in the near-infrared range, two small peaks can be found around 1500 and 2000 nm. We think these two absorption peaks are owing to the lattice vibration absorption peak from the interaction of In_2S_3 and TiO_2. Moreover, the Tauc Plot shown in Figure 4b presents the bandgaps of In_2S_3-TiO_2, In_2S_3, and TiO_2. It was found that, after annealing treatment, the bandgap of TiO_2 used here is around 3.32 eV, which is a bit bigger than data from the literature[39]. The bandgap of In_2S_3 is around 2.3 eV, which is consistent with the literature[36]. Furthermore, the two bandgaps in In_2S_3-TiO_2 are close to individual In_2S_3 and TiO_2.

Based on the published works, the valence band and conduction band of In_2S_3 are around 1.32 and –0.98 eV, respectively,[29,30] while those of TiO_2 are around 2.84 and –0.42 eV, respectively.[31,32] Subsequently, we have drawn a schematic diagram of the band alignment of the as-prepared In_2S_3-TiO_2, as shown in Figure 5. As the bandgap of as-prepared TiO_2 (3.32 eV) and the published TiO_2 (3.26 eV) is different, we take this difference (~0.06 eV) into account by using fuzzy values to define the band positions of TiO_2. The valence band of TiO_2 is in a range of 2.9 to 2.78 eV, while the conduction band of TiO_2 change from –0.36 eV to –0.48 eV. In this case, the conduction band position

DOI: 10.14102/j.cnki.0254-5861.2021-0046

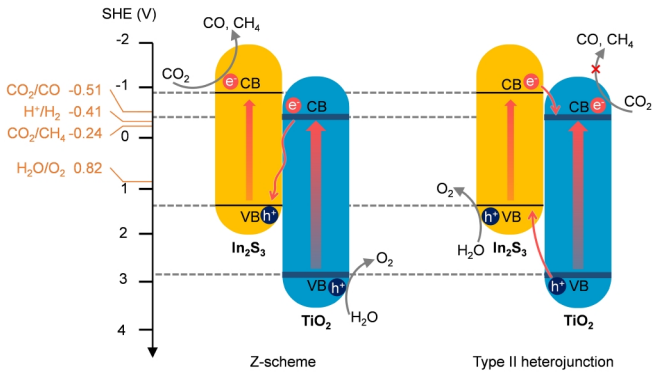

Figure 5. Schematic diagram of the band alignment of the as-prepared In_2S_3-TiO_2 in Z-scheme structure or type II heterojunction structure. CB indicates conduction band. VB indicates valence band. The Standard Hydrogen Electrode (SHE) is used as the reference. The standard reaction potentials of CH_4, CO, H_2, and O_2 at pH = 7 are adapted from the literature.[41-43]

of TiO_2 should be no more than –0.48 eV, which is still lower than the standard reaction potential of CO, –0.51 V. Also, the valence band of In_2S_3 is more negative than the standard reaction potential of O_2 evolution. Therefore, CO is hard to be produced with the electrons from the conduction band of TiO_2 *via* the charge transfer of a type II heterojunction structure, which is consistent with the literature in Table S1. However, we do detect CO and CH_4 in the measurements. We believe that the photo-generated charges within the as-prepared In_2S_3-TiO_2 photocatalyst are transferred in a Z-scheme route. As noted earlier, in a Z-scheme, the electrons at the conduction band of In_2S_3 have a higher energy level than that of TiO_2, thus presenting a higher capability to drive the CO_2R.

n CONCLUSION

In summary, we reported an In_2S_3-TiO_2 composite photocatalyst for CO_2R. Driven by the concentrated natural sunlight, this photocatalytic CO_2R system reached a solar to fuel efficiency of 0.002%. The average evolution rates of H_2, CO, and C_2H_5OH reached 262.2, 73.9, and 27.56 $\mu mol \cdot h^{-1} \cdot g^{-1}$, respectively. The photocatalytic CO_2R reaction at 170 °C of In_2S_3-TiO_2 lasted more than 4 hours under the concentrated natural sunlight, but less than 1 hour at 250 ℃ under the simulated sunlight. We also find that In_2S_3 and TiO_2 should be combined for reducing CO_2 to CO. Considering the band alignment of In_2S_3-TiO_2, we believe that the In_2S_3 and TiO_2 formed a Z-scheme structure for CO_2R.

n EXPERIMENTAL

Photocatalysts Preparation. TiO_2-In_2S_3 was synthesized by adding In_2S_3 onto a commercial TiO_2 (anatase, Macklin). Before preparing the composite catalyst, TiO_2 was firstly annealed in a muffle furnace at 300 °C for 3 hours under an air atmosphere. Next, 0.6 mmol $In(NO_3)_3 \cdot xH_2O$, 1.8 mmol $Na_2S \cdot 9H_2O$, and 100 mg of annealed TiO_2 were added into 45 mL aqueous nitric acid solution (0.01 mol/L). After ~30 min, the mixed aqueous solution was transferred into an autoclave with a 100 mL inner volume and heated at 180 °C for 16 hours. Next, the obtained sediments in the autoclave were washed with deionized water and ethanol, and then dried in a vacuum drying oven. Moreover, the In_2S_3 used in the control experiment was prepared via a solid-state reaction.[43] 0.6 mmol $In(NO_3)_3 \cdot xH_2O$ and 1.2 mmol thiourea were uniformly mixed in an agate, and then annealed in the air at 220 °C for 5 minutes with a heating rate of 10 °C/min. After being cooled down to room temperature, the as-obtained powder was washed three times with deionized water and ethanol to remove any impurities. Finally, the as-prepared In_2S_3 was dried in a vacuum oven until the color changed to orange-red.

The crystal structure and morphology of as-prepared samples were analyzed by X-ray Diffractometer (XRD, X'Pert PRO MPD, PANalytical) and Transmission Electron Microscopy (TEM, FEI Tecnai G2 F30). The Energy Dispersive X-ray (EDX) mapping analysis of composites was conducted on the same TEM. The optical properties were measured by a UV-vis-NIR spectrophotometer (Agilent Cary 5000, USA).

Photocatalytic CO_2R System. For the CO_2R measurements under concentrated natural sunlight, 0.02 g photocatalyst was put into a spherical reactor with a Fresnel lens (490 cm^2). The reaction area was 1 cm^2. Before being injected into the reactor, CO_2 was humidified by water at 25 °C. The flow rate of CO_2 is kept at 20 sccm. During the measurements, the reactor was heated independently by the concentrated natural sunlight. The gas products (H_2, CO, and hydrocarbons) were online detected by a Gas Chromatography (GC, Shimadzu), including two flame ionization detectors (FID) and one thermal conductivity detector (TCD). Gas flowing from the reactor was sampled every 20 minutes. All of the liquid products were collected in a self-made condensing tube and were detected by a high-performance liquid chromatography (HPLC, Agilent 1260), including a column (Aminex HPX 87-H) from Bio-Rad and a refractive index detector (RID). The light intensity was measured by a PC-2-T1 solar radiation monitoring system (Jin Zhou Sunshine Meteorological Technology Co., Ltd.). We also measured the photocatalytic performance of photocatalyst under simulated sunlight (xenon lamp) as the control experiment. 0.02 g photocatalyst was put into a quartz photocatalytic reactor and distributed into a flat surface with a diameter of 1 cm. An electric heating panel was used to maintain the temperature of the reactor, which was carried out at 150, 170, 200, and 250 °C, respectively. Similar to the measurement outdoor, the CO_2 flow rate is kept at 20 sccm.

n ACKNOWLEDGEMENTS

This research was supported by the National Natural Science Foundation of China (51906199), and China Postdoctoral Science Foundation Funded Project (2019M663703).

n AUTHOR CONTRIBUTION

Y. Liu and F. Yu have contributed equally to this work.

n AUTHOR INFORMATION

Corresponding author. Email: yaliu0112@xjtu.edu.cn

n COMPETING INTERESTS

The authors declare that they have no known competing financial interests or personal relationships that may affect the work reported in this paper.

n ADDITIONAL INFORMATION

DOI: 10.14102/j.cnki.0254-5861.2021-0046

Supplementary information is available for this paper at http://manu30.magtech.com.cn/jghx/EN/10.14102/j.cnki.0254-5861.2021-0046

For submission: https://mc03.manuscriptcentral.com/cjsc

n REFERENCES

(1) Albero, J.; Peng, Y.; García, H. Photocatalytic CO_2 reduction to C2+ products. *ACS Catal.* **2020**, 10, 5734–5749.

(2) Tang, H.; Xia, Z.; Chen, R.; Liu, Q.; Zhou, T. Oxygen doped g-C_3N_4 with nitrogen vacancy for enhanced photocatalytic hydrogen evolution. *Chem. Asian J.* **2020**, 15, 3456–3461.

(3) Zhang, H. X.; Hong, Q. L.; Li, J.; Wang, F.; Huang, X.; Chen, S.; Tu, W.; Yu, D.; Xu, R.; Zhou, T.; Zhang, J. Isolated square-planar copper center in boron imidazolate nanocages for photocatalytic reduction of CO_2 to CO. *Angew. Chem. Int. Ed.* **2019**, 58, 11752–11756.

(4) Xiong, X.; Mao, C.; Yang, Z.; Zhang, Q.; Waterhouse, G. I. N.; Gu, L.; Zhang, T. Photocatalytic CO_2 reduction to CO over Ni single atoms supported on defect-rich zirconia. *Adv. Energy Mater.* **2020**, 10, 2002928.

(5) Zhang, Y.; Xia, B.; Ran, J.; Davey, K.; Qiao, S. Z. Atomic-level reactive sites for semiconductor-based photocatalytic CO_2 reduction. *Adv. Energy Mater.* **2020**, 10, 1903879.

(6) Liu, M. Y.; Liu, Q. Y.; Zheng, Y. F.; Lin, G. L.; Song, X. C. $BiIO_4$ nanoflakes for the degradation of phenol under simulated solar light irradiation. *Chin. J. Struc. Chem.* **2019**, 38, 1404–1413.

(7) Liu, Y.; Guo, L. On factors limiting the performance of photoelectrochemical CO_2 reduction. *J. Chem. Phys.* **2020**, 152, 100901.

(8) Dai, X.; Chen, L.; Li, Z.; Li, X.; Wang, J.; Hu, X.; Zhao, L.; Jia, Y.; Sun, S. X.; Wu, Y.; He, Y. CuS/$KTa_{0.75}Nb_{0.25}O_3$ nanocomposite utilizing solar and mechanical energy for catalytic N_2 fixation. *J. Colloid Interface Sci.* **2021**, 603, 220–232.

(9) Chen, L.; Dai, X.; Li, X.; Wang, J.; Chen, H.; Hu, X.; Lin, H.; He, Y.; Wu, Y.; Fan, M. A novel Bi_2S_3/$KTa_{0.75}Nb_{0.25}O_3$ nanocomposite with high efficiency for photocatalytic and piezocatalytic N_2 fixation. *J. Mater. Chem. A* **2021**, 9, 13344–13354.

(10) Chen, L.; Zhang, W.; Wang, J.; Li, X.; Li, Y.; Hu, X.; Zhao, L.; Wu, Y.; He, Y. High piezo/photocatalytic efficiency of Ag/Bi_5O_7I nanocomposite using mechanical and solar energy for N_2 fixation and methyl orange degradation. *Green Energy Environ.* **2021**. doi: 10.1016/j.gee.2021.04.009.

(11) Cheng, C.; Mao, L.; Shi, J.; Xue, F.; Zong, S.; Zheng, B.; Guo, L. $NiCo_2O_4$ nanosheets as a novel oxygen-evolution-reaction cocatalyst in situ bonded on the g-C_3N_4 photocatalyst for excellent overall water splitting. *J. Mater. Chem. A* **2021**, 9, 12299–12306.

(12) Cheng, C.; Shi, J.; Wen, L.; Dong, C. L.; Huang, Y. C.; Zhang, Y.; Zong, S.; Diao, Z.; Shen, S.; Guo, L. Disordered nitrogen-defect-rich porous carbon nitride photocatalyst for highly efficient H_2 evolution under visible-light irradiation. *Carbon* **2021**, 181, 193–203.

(13) Lin, H.; Chen, C.; Zhou, T.; Zhang, J. Two-dimensional covalent-organic frameworks for photocatalysis: the critical roles of building block and linkage. *Sol. RRL* **2021**, 5, 2000458.

(14) Liu, S. H.; Li, Y.; Ding, K. N.; Chen, W. K.; Zhang, Y. F.; Lin, W. Mechanism on carbon vacancies in polymeric carbon nitride for CO_2 photoreduction. *Chin. J. Struct. Chem.* **2020**, 39, 2068–2076.

(15) Li, Y.; Li, B.; Zhang, D.; Cheng, L.; Xiang, Q. Crystalline carbon nitride supported copper single atoms for photocatalytic CO_2 reduction with nearly 100% CO selectivity. *ACS Nano* **2020**, 14, 10552–10561.

(16) Cheng, C.; Dong, C. L.; Shi, J.; Mao, L.; Huang, Y. C.; Kang, X.; Zong, S.; Shen, S. Regulation on polymerization degree and surface feature in graphitic carbon nitride towards efficient photocatalytic H_2 evolution under visible-light irradiation. *J. Mater. Sci. Technol.* **2022**, 98, 160–168.

(17) Zhang, Y.; Shi, J.; Huang, Z.; Guan, X.; Zong, S.; Cheng, C.; Zheng, B.; Guo, L. Synchronous construction of CoS_2 in-situ loading and S doping for g-C_3N_4: enhanced photocatalytic H_2-evolution activity and mechanism insight. *Chem. Eng. J.* **2020**, 401, 126135.

(18) Kho, E. T.; Tan, T. H.; Lovell, E.; Wong, R. J.; Scott, J.; Amal, R. A review on photo-thermal catalytic conversion of carbon dioxide. *Green Energy Environ.* **2017**, 2, 204–217.

(19) Zhang, F.; Li, Y. H.; Qi, M. Y.; Yamada, Y. M. A.; Anpo, M.; Tang, Z. R.; Xu, Y. J. Photothermal catalytic CO_2 reduction over nanomaterials. *Chem. Catal.* **2021**, 1, 272–297.

(20) Mateo, D.; Cerrillo, J. L.; Durini, S.; Gascon, J. Fundamentals and applications of photo-thermal catalysis. *Chem. Soc. Rev.* **2021**, 50, 2173–2210.

(21) Zhang, Z.; Gao, Z.; Liu, H.; Abanades, S.; Lu, H. High photo thermally active Fe_2O_3 film for CO_2 photoreduction with H_2O driven by solar light. *ACS Appl. Energy Mater.* **2019**, 2, 8376–8380.

(22) Fang, X.; Gao, Z.; Lu, H.; Zhang, Z. Boosting CO_2 photoreduction activity by large fresnel lens concentrated solar light. *Catal. Commun.* **2019**, 125, 48–51.

(23) Ma, D.; Liu, W.; Chen, Q.; Jin, Z.; Zhang, Y.; Huang, J.; Zhang, H.; Peng, F.; Luo, T. Titanium-oxo-clusters precursors for preparation of In_2S_3/TiO_2 heterostructure and its photocatalytic degradation of tetracycline in water. *J. Solid State Chem.* **2021**, 293, 121791.

(24) Yang, Y.; Cheng, B.; Yu, J.; Wang, L.; Ho, W. TiO_2/In_2S_3 S-scheme photocatalyst with enhanced H_2O_2-production activity. *Nano Res.* **2021**.

(25) Wang, L.; Huang, G.; Zhang, L.; Lian, R.; Huang, J.; She, H.; Liu, C.; Wang, Q. Construction of TiO_2-covalent organic framework Z-scheme hybrid through coordination bond for photocatalytic CO_2 conversion. *J. Energy Chem.* **2022**, 64, 85–92.

(26) She, H.; Ma, X.; Chen, K.; Liu, H.; Huang, J.; Wang, L.; Wang, Q. Photocatalytic H_2 production activity of TiO_2 modified by inexpensive $Cu(OH)_2$ cocatalyst. *J. Alloys Compd.* **2020**, 821, 153239.

(27) Wu, Z.; Yuan, X.; Zeng, G.; Jiang, L.; Zhong, H.; Xie, Y.; Wang, H.; Chen, X.; Wang, H. Highly efficient photocatalytic activity and mechanism of Yb^{3+}/Tm^{3+} codoped In_2S_3 from ultraviolet to near infrared light towards chromium (VI) reduction and rhodamine B oxydative degradation. *Appl. Catal. B* **2018**, 225, 8–21.

(28) Gao, W.; Liu, W.; Leng, Y.; Wang, X.; Wang, X.; Hu, B.; Yu, D.; Sang, Y.; Liu, H. In_2S_3 nanomaterial as a broadband spectrum photocatalyst to display significant activity. *Appl. Catal. B* **2015**, 176–177, 83–90.

(29) Li, Y.; Luo, S.; Wei, Z.; Meng, D.; Ding, M.; Liu, C. Electrodeposition technique-dependent photoelectrochemical and photocatalytic properties of an In_2S_3/TiO_2 nanotube array. *Phys. Chem. Chem. Phys.* **2014**, 16, 4361–4368.

(30) Huang, W.; Gan, L.; Yang, H.; Zhou, N.; Wang, R.; Wu, W.; Li, H.; Ma, Y.; Zeng, H.; Zhai, T. Controlled synthesis of ultrathin 2D β-In_2S_3 with broadband photoresponse by chemical vapor deposition. *Adv. Funct. Mater.* **2017**, 27, 1702448.

(31) Chao, G.; Li, J.; Shan, Z.; Huang, F.; Shen, H. Preparation and visible-light photocatalytic activity of In_2S_3/TiO_2 composite. *Mater. Chem. Phys.* **2010**, 122, 183–187.

(32) Sarkar, S. K.; Kim, J. Y.; Goldstein, D. N.; Neale, N. R.; Zhu, K.; Elliot, C. M.; Frank, A. J.; George, S. M. In_2S_3 atomic layer deposition and its application as a sensitizer on TiO_2 nanotube arrays for solar energy conversion. *J. Phys. Chem. C* **2010**, 114, 8032–8039.

(33) Huang, G.; Shen, Q.; Ma, X.; Zhong, J.; Chen, J.; Huang, J.; Wang, L.; She, H.; Wang, Q. Preparation of an In_2S_3/TiO_2 heterostructure for enhanced activity in carbon dioxide photocatalytic reduction.

DOI: 10.14102/j.cnki.0254-5861.2021-0046

ChemPhotoChem **2021**, 5, 438–444.
(34) Chen, L. Y.; Zhang, Z. D.; Wang, W. Z. Self-assembled porous 3D flowerlike β-In_2S_3 structures: synthesis, characterization, and optical properties. *J. Phys. Chem. C* **2008**, 112, 4117–4123.
(35) An, X.; Tang, Q.; Lan, H.; Liu, H.; Qu, J. Polyoxometalates/TiO_2 fenton-like photocatalysts with rearranged oxygen vacancies for enhanced synergetic degradation. *Appl. Catal. B* **2019**, 244, 407–413.
(36) Khanchandani, S.; Kundu, S.; Patra, A.; Ganguli, A. K. Band gap tuning of ZnO/In_2S_3 core/shell nanorod arrays for enhanced visible-light-driven photocatalysis. *J. Phys. Chem. B* **2013**, 117, 5558–5567.
(37) Chen, L. Y.; Zhang, Z. D.; Wang, W. Z. Self-assembled porous 3D flowerlike β-In_2S_3 structures: synthesis, characterization, and optical properties. *J. Phys. Chem. C* **2008**, 112, 4117–4123.
(38) Xu, J.; Luo, B.; Gu, W.; Jian, Y.; Wu, F.; Tang, Y. B.; Shen, H. Fabrication of In_2S_3/$NaTaO_3$ composites for enhancing the photocatalytic activity toward the degradation of tetracycline. *New J. Chem.* **2018**, 42, 5052–5058.
(39) Liu, Y.; Jiang, J.; Xu, Q.; Li, M.; Guo, L. Photoelectrochemical performance of CdS nanorods grafted vertically aligned TiO_2 nanorods. *Mater. Res. Bull.* **2013**, 48, 4548–4554.
(40) Matsubara, Y. Standard electrode potentials for the reduction of CO_2 to CO in acetonitrile-water mixtures determined using a generalized method for proton-coupled electron-transfer reactions. *ACS Energy Letters* **2017**, 2, 1886–1891.
(41) Wu, J.; Huang, Y.; Ye, W.; Li, Y. CO_2 reduction: from the electrochemical to photochemical approach. *Adv. Sci.* **2017**, 4, 1700194.
(42) Sun, Z.; Ma, T.; Tao, H.; Fan, Q.; Han, B. Fundamentals and challenges of electrochemical CO_2 reduction using two-dimensional materials. *Chem* **2017**, 3, 560–587.
(43) Wang, L.; Zhao, B.; Wang, C.; Sun, M.; Yu, Y.; Zhang, B. Thermally assisted photocatalytic conversion of CO_2-H_2O to C_2H_4 over carbon doped In_2S_3 nanosheets. *J. Mater. Chem. A* **2020**, 8, 10175–10179.

Received: November 25, 2021
Accepted: December 10, 2021
Published: January 13, 2022

DOI: 10.14102/j.cnki.0254-5861.2021-0046